

## FEM-BASED DEVELOPMENT OF NOVEL BACK-CONTACT PV MODULES WITH ULTRA-THIN SOLAR CELLS

Andreas J. Beinert<sup>1,2</sup>, Roman Leidl<sup>3</sup>, Paul Sommeling<sup>4</sup>, Ulrich Eitner<sup>1</sup> and Jarir Aktaa<sup>2</sup>

<sup>1</sup>Fraunhofer Institute for Solar Energy Systems ISE, Heidenhofstraße 2, 79110 Freiburg, Germany

<sup>2</sup>Karlsruhe Institute of Technology (KIT), Institute for Applied Materials, Hermann-von-Helmholtz-Platz 1, 76344 Eggenstein-Leopoldshafen, Germany

<sup>3</sup>AIT Austrian Institute of Technology GmbH, Giefinggasse 2, 1210 Vienna, Austria

<sup>4</sup>Energy Research Centre of the Netherlands (ECN), Westerduinweg 3, 1755 LE Petten, The Netherlands

Corresponding author: Andreas J. Beinert | Phone: +49 (0)761 4588 5630 | E-mail: Andreas.Beinert@ise.fraunhofer.de

**ABSTRACT:** With the availability of ultra-thin back contact solar cells, the question arises if they can be integrated into PV modules. Particularly the single-side metallization and joint architecture of back contact solar cells may cause critical stress. We develop a three-dimensional finite element model of a frameless 60-cell module with an electrically conductive backsheet to simulate the cell stress in terms of mechanical push load. The FEM model is validated by mechanical load tests of frameless modules. With the validated model we perform a variation of the cell and encapsulant thickness from 80  $\mu\text{m}$  to 180  $\mu\text{m}$  and 200  $\mu\text{m}$  to 460  $\mu\text{m}$ , respectively. Moreover we compare three different encapsulant materials, one Ethylene-vinyl acetate copolymer (EVA), one thermoset Polyolefin elastomer (POE-TS), one thermoplastic POE (POE-TP) and two different electrically conductive adhesives. The combination of 460  $\mu\text{m}$  thick EVA and 180  $\mu\text{m}$  cells shows the lowest first principal stress  $\sigma_1$  which, however, is far above the measured critical fracture stress of 134 MPa for the MWT cells used. We then modify the FEM model to simulate a framed glass-foil as well as a framed and frameless glass-glass module with the same material combination, 80  $\mu\text{m}$  cells and 200  $\mu\text{m}$  encapsulant. The framed glass-foil module shows a by 54% reduced deflection and a stress of 114 MPa, which is much smaller than without a frame (296 MPa). The lowest value is achieved for the framed glass-glass module with 66 MPa. An interesting finding from the thickness variation is, that for cells below about 110  $\mu\text{m}$  thickness the stress increases with increasing encapsulant thickness, while for thicker cells the stress decreases.

**Keywords:** thin solar cells, thermomechanical stress, FEM modeling, material characterization, PV module design

### 1 INTRODUCTION

Since the development of novel module designs is an expensive, time-consuming process, virtual prototyping by the finite element method (FEM) is a convenient way for identifying robust PV module designs. [1] From a mechanical point of view, the mechanical load is a crucial test in the IEC61215 [2] sequence for novel module designs. In this work we investigate the potential of reducing the encapsulant and solar cell thickness in PV modules with back contact solar cells connected by electrically conductive adhesives (ECA) and an electrically conductive backsheet. This concept has been investigated before with a focus on the thermomechanical challenges due to temperature cycling e.g. [3–5]. In this work, we develop a 3-dimensional FEM-model which is capable of resolving the stress which arises from lamination and mechanical load in great detail. The FEM-model is validated by a mechanical load test. With the validated FEM-model we compare six different material combinations as well as different layer thicknesses of the back contact solar cells and encapsulant.

### 2 METHOD

The work consists of three interacting parts (figure 1). The main part is the FEM-modelling, which gets input from the material characterization. The results of the FEM-simulation are compared with experimental results from 4-line cell bending tests in terms of cell fracture probability and validated by mechanical load tests on full-size modules.

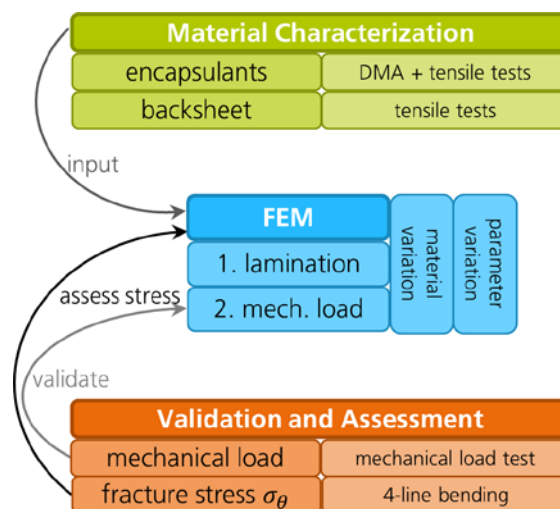


**Figure 1:** Flowchart of work.

#### 2.1 Material characterization

Since the material parameters of the encapsulants are crucial for the thermomechanical behavior of the laminate, we measure the Young's modulus and Poisson's ratio. We use a dynamic mechanical analyzer (DMA) to measure the Young's modulus for the temperature range of  $-100\text{ }^{\circ}\text{C}$ ... $+160\text{ }^{\circ}\text{C}$ . The Poisson's ratio is measured by a tensile tester using an optical extensometer at ambient temperature. Additionally we measure the backsheets Young's modulus at ambient temperature by a tensile tester. We investigate one Ethylene-vinyl acetate copolymer (EVA), one thermoset Polyolefin elastomer (POE-TS), one thermoplastic POE (POE-TP) and one electrically conductive backsheet. The corresponding results are shown in table 1 and figure 2.

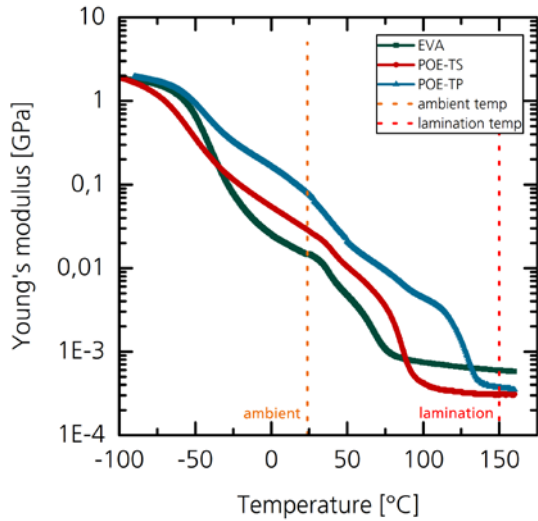


**Figure 2:** Measured temperature dependent Young's modulus of the three different encapsulants.

### 2.2 Finite Element model

Because of the large aspect ratio of the solar cell edge length to its thickness, mechanical modelling of PV modules is a challenging task. In order to minimize the computational effort, we exploit the symmetry of the PV laminate by modelling a quarter laminate. Additionally we apply the sub-modelling method, which allows separating the model into two problems: the computation of the displacement in the global-model and the computation of the stress in the sub-model with a minimized geometry and finer mesh, more details in [6]. The global-model consists of a 60-cell unframed PV laminate with monocrystalline full-square 156x156 mm<sup>2</sup> back contact solar cells. The overall dimension of the PV laminate is 1.61x0.98 m<sup>2</sup>. The target thickness of each layer and the materials used are shown in table 2.

**Table 1:** Material properties used in the FEM-model. \*: provided by manufacturer; +: measured.

Material	Density $\rho$ [kg/m <sup>3</sup> ]	Young's modulus $E$ [GPa]	Poisson's ratio $\nu$ [-]	CTE $\alpha$ [10 <sup>-6</sup> K <sup>-1</sup> ]
Solar glass	2530*	74*	0.24*	9.5*
EVA	820 <sup>+</sup>	$T$ -dep. <sup>+</sup>	0.22 <sup>+</sup>	270 [7]
POE-TS	941 <sup>+</sup>	$T$ -dep. <sup>+</sup>	0.31 <sup>+</sup>	270 [7]
POE-TP	865 <sup>+</sup>	$T$ -dep. <sup>+</sup>	0.26 <sup>+</sup>	270 [7]
Cz-silicon	2329 [7]	Elasticity Matrix [7]		$T$ -dep. [8, 9]
ECAI	3950*	$T$ -dep. <sup>+</sup>	0.3*	46*
ECAII	3600*	$T$ -dep. <sup>+</sup>	0.3*	$T$ -dep.*
Back sheet	1315*	6.36 <sup>+</sup>	0.29 [7]	50.4 [7]
Al	2700 [10]	70 [10]	0.33 [10]	23 [10]
Rubber inlay	67*	0.0074*	0.3*	769*

The sub-model consists of the cell matrix embedded in the encapsulants and 31 ECA contact joints per cell. The result of the global model is transferred as boundary

and initial conditions to the sub-model. A rectangular mapped mesh is used. In the sub-model the number of 180 elements per cell edge is increased by 10%. Also the amount of elements per layer height is increased for each layer individually.

The model is computed in two successive steps. First the lamination process by cooling down from 150 °C to 23.8 °C. Secondly the mechanical push load of 2400 Pa is applied onto the thermally stressed module at 23.8 °C. In the first step the laminate is not mounted, while in the second step six laminate clamps are used. For this purpose, the clamps are implemented by an additional sub-model to the global-model.

From a FEM pre-study we find that the load application pattern has a significant impact on the module deflection. Therefore we implement the used vacuum cups of the test stand by a two-dimensional spatially resolved Gaussian distribution, shown in figure 3. We assume the load magnitude to be equal for each vacuum cup. We validate the deflection by mechanical load tests on full-size modules. With the validated model we compare six different material combinations (three encapsulants and two ECA's). Moreover we conduct a parameter variation study of the thickness of the solar cell and the encapsulant for all combinations. For the material combination with the least stress we modify the FEM model to simulate a framed module as well as a glass-glass setup with and without frame.

**Table 2:** PV module materials used in the FEM model with corresponding thickness (target thickness in bold).

Layer	Material	Thickness [ $\mu$ m]
Front glass	solar glass	3200
Encapsulant	EVA, POE-TS, POE-TP	100, <b>200</b> , 300, 460
Solar cells	monocrystalline silicon	<b>80</b> , 120, 180
ECA	ECAI, ECAII	200
Backsheet	Cu-PA-PET-PVF	380
Frame	Aluminum with rubber inlay	1500

### 2.3 Validation

For the validation, we measure the deflection of three frameless PV-modules with 180  $\mu$ m thick MWT-cells during several mechanical load cycles. In pre-tests we find that for higher loads the laminate slips out of the laminate clamps. Therefore the test load is limited to 1000 Pa. The deflection is measured by four laser sensors with a measurement resolution of 1 mm. Figure 3 shows the positions of the laser sensors.

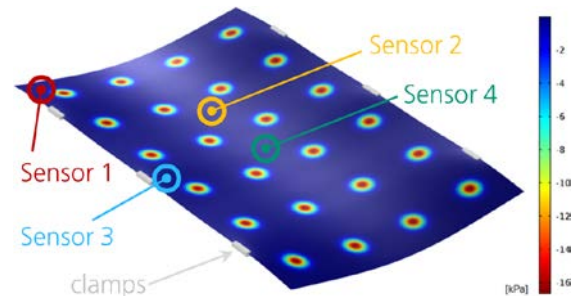


**Figure 3:** Gaussian load distribution of the vacuum cups at 1000 Pa load, with position of the distance sensors.

### 3 RESULTS

#### 3.1 Fracture stress by 4-line-bending

In order to assess the criticality of the results from the FEM-model, we determined the characteristic fracture stress on the rear side of ten industrial MWT-cells, used in the validation experiment by a four-line-bending test. The results are presented in figure 4 as a Weibull plot [11, 12]. We obtain a characteristic fracture stress of 134 MPa. Since the fracture stress of silicon is a tensile stress, we evaluate in the FEM study the first principal stress  $\sigma_1$ , which is the tensile stress equivalent. More precisely, the highest stress values arise at the contact joint of the contact pad and the solar cell. Thus we evaluate the mean first principal stress  $\bar{\sigma}_1$  over this contact area at the contact joint with maximum first principal stress  $\sigma_1$ .

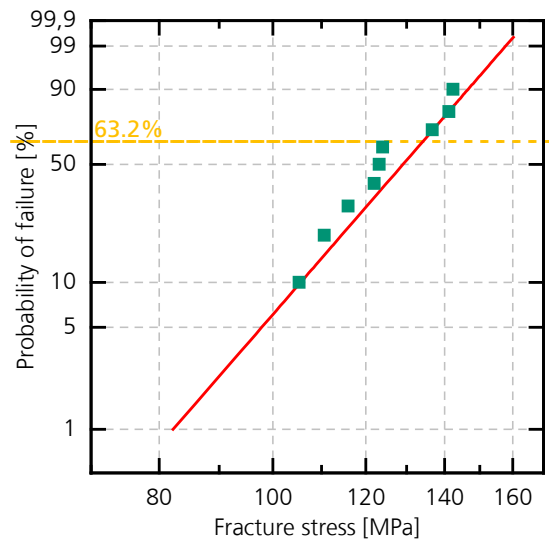


**Figure 4:** Weibull-plot for 4-line bending fracture tests of ten MWT cells. The dashed yellow line is the value at which the characteristic fracture stress is determined.

#### 3.2 FEM-model validation

Due to their position close to the clamps, sensor 1 and 3 show minor deflection values, consequently the uncertainty of the laser sensor measurement is fairly large compared to the deflection. Therefore we evaluate only sensor 2 and 4 for the validation. The deflection measured by sensor 4 in dependence on the applied load is shown in figure 5 together with the result of the FEM-model. A similar graph is obtained for sensor 2 (not shown). The FEM results lie within the upper third of the experimental data for both sensors. This slight underestimation of the deflection might be due to the assumption of equal load of each vacuum cup. Overall speaking, the FEM results match the experimental data reasonably well. Therefore an equal load of each vacuum cup is considered to be a valid assumption for this work. The deflection values at 0 Pa load represent the deflection due to gravity. According to the FEM results the gravitational deflection is about 3 mm.

The experimental values of deflection are only available up to 1000 Pa, but the mechanical load test according to IEC61215 [2] is carried out at 2400 Pa, therefore, we extrapolate the experimental data using a linear fit of the data of all modules. This is a reasonable approximation since previous results show a linear

behavior of the deflection in this range [13]. At 2400 Pa the FEM results deviate by about 10 mm from the extrapolated data, which corresponds to about 10 % and is equal to the scattering of the experimental data.

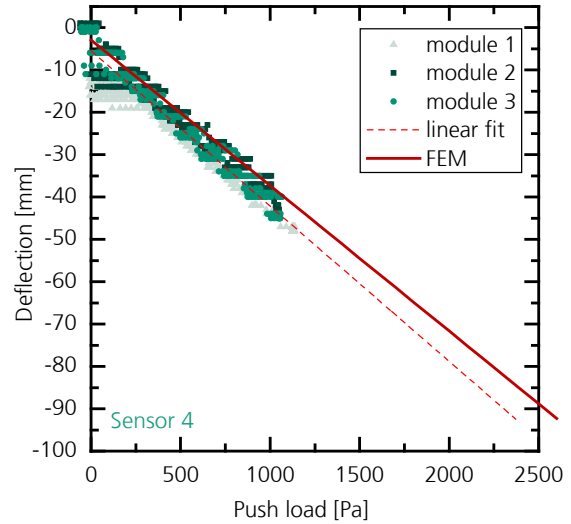


**Figure 5:** Deflection-load curve of experimental data (symbols) with extrapolated linear fit (dashed line) and FEM results (solid line) for the distance sensor 4.

We investigate the tested modules after different load levels for new cracks by electroluminescence (EL) imaging. The obtained crack pattern coincides very well with the stress pattern obtained from the FEM simulation. Figure 6 shows exemplarily the EL-image of validation module 3 after 1000 Pa push load overlaid with the corresponding FEM result. We therefore consider the FEM model to be sufficiently valid.

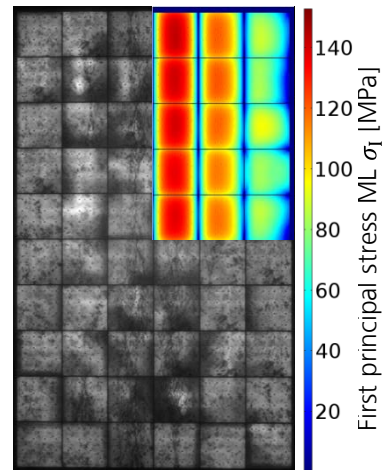


**Figure 6:** Electroluminescence image of validation module 3 after 1000 Pa push load overlaid with the FEM result at the same load.

#### 3.3 Lamination

Due to the mismatch of the coefficients of thermal expansion of the different layers within the PV laminate (see table 1), the cooling down after lamination leads to thermomechanical stress. We set the lamination temperature of 150 °C as the stress-free temperature. Therefore the stress increases with decreasing temperature. With the backsheets contracting stronger than the front glass, the module slightly bends, showing a

convex shape from the sunny side. Accordingly, the solar cell deformation is also convex and the front side is in tensile mode. Thus, the mean first principal stress  $\bar{\sigma}_1$  is evaluated on the front side by taking the mean stress value over the contact pad area at its position on the front side. Figure 7 shows the maximum mean first principal stress  $\bar{\sigma}_1$  for all six material combinations with the target material layer thicknesses given in table 2. All variations are far below the characteristic fracture stress  $\sigma_\theta$ , hence we do not expect any cell cracking after lamination.

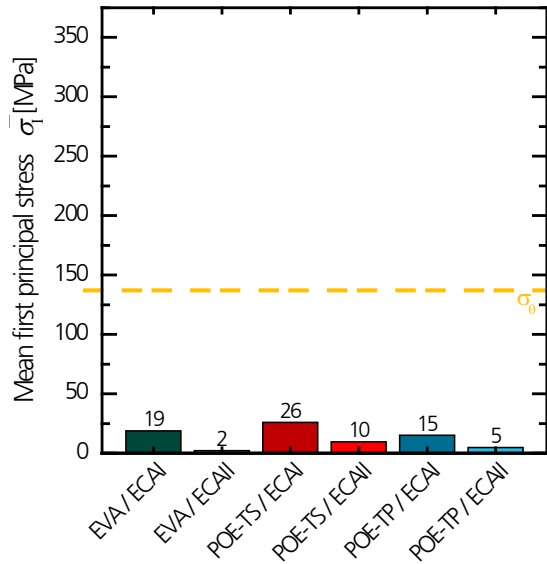


**Figure 7:** Mean first principal stress  $\bar{\sigma}_1$  on the front side of the solar cells after lamination. The dashed yellow line indicates the characteristic fracture stress  $\sigma_\theta$ .

### 3.4 Mechanical load

The bending of the PV laminate due to 2400 Pa mechanical pressure load leads to tensile stress on the rear side of the solar cells. Exemplarily, figure 8 shows the first principal stress  $\sigma_1$  on the rear side of the solar cells at 2400 Pa pressure load for the combination of EVA with ECAII with the target thickness. The pattern of the contact joints is clearly visible due to the higher stress values, because the contact pads apply an additional strain to the solar cell.

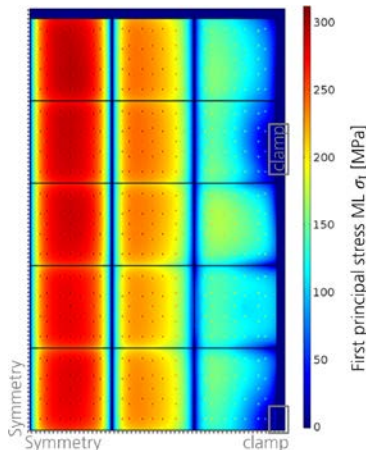


**Figure 8:** First principal stress  $\sigma_1$  on the rear side of the solar cells at 2400 Pa mechanical push load for the combination of EVA with ECAII with target thickness.

The dependence of the mean first principal stress  $\bar{\sigma}_1$  on the cell and encapsulant thickness is depicted in figure 9 and figure 10, respectively. For the cell thickness variation we use a EVA thickness of 200  $\mu\text{m}$ . For all material combinations the deflection decreases between 8 - 10%, depending on the combination, with increasing cell thickness (not shown). The same behavior is obtained for the stress decreases. The lowest stress is achieved by the combination of EVA (200  $\mu\text{m}$ ) with ECAI and 180  $\mu\text{m}$  cell thickness. However with 260 MPa, the value is about two times above the characteristic fracture stress  $\sigma_\theta$  of 134 MPa. Comparing this to standard solar cells, which have a higher characteristic fracture stress  $\sigma_\theta$  of about 200 MPa [14], the value is still in a critical range. This corresponds well with previous findings for a clamped frameless common PV module with 460  $\mu\text{m}$  EVA [6]. Decreasing the cell thickness to the target thickness of 80  $\mu\text{m}$  increases the stress between 4% and 12%, depending on the material combination. EVA with ECAI shows the largest increase.

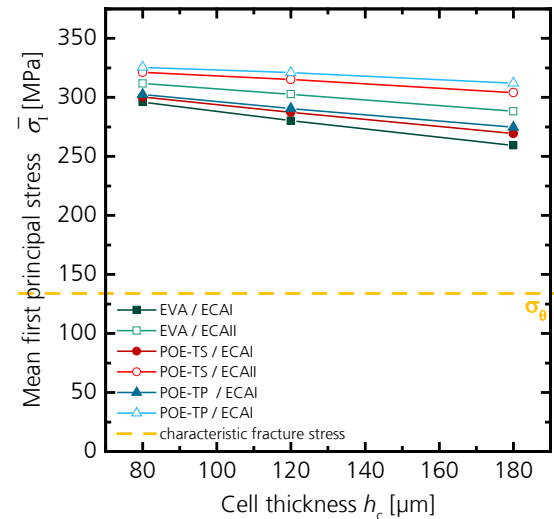


**Figure 9:** Mean first principal stress  $\bar{\sigma}_1$  on rear side of the solar cells at 2400 Pa pressure load for different solar cells thickness with an encapsulant thickness of 200  $\mu\text{m}$ .

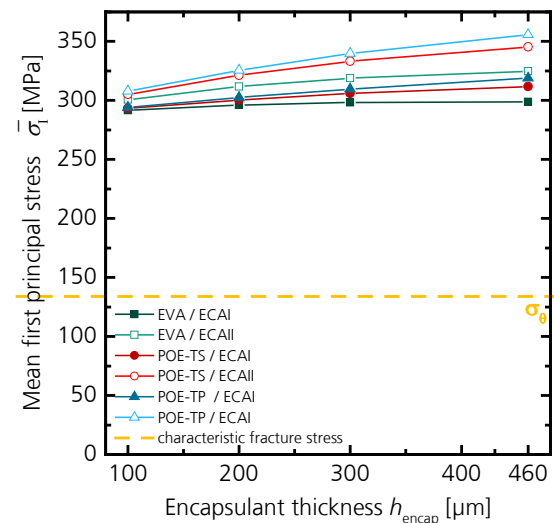


**Figure 10:** Mean first principal stress  $\bar{\sigma}_1$  on the rear side of the solar cells at 2400 Pa pressure load for different encapsulant thickness with 80  $\mu\text{m}$  thin solar cells.



Surprisingly, the mean first principal stress  $\bar{\sigma}_1$  increases with increasing encapsulant thickness for 80  $\mu\text{m}$  thick cells. The reason for this behavior lies in the coupling of the cells to the backsheet through the contact pads. So the strain in the solar cells is directly coupled to the strain in the backsheet. Moreover, the strain in the backsheet due to push load increases with increasing module thickness, assuming a constant bending radius on the glass surface, i.e. the bending radius of the backsheet increases for an increasing module thickness. Now, with increasing encapsulant thickness, the module thickness increases and so does the strain in the backsheet. Simultaneously the difference between the strain of the solar cells and the strain of the backsheet increases. On the other hand, the module bend decreases by 4 - 6% for an increasing encapsulant thickness due to higher strain in the encapsulant and a higher laminate bending stiffness, which causes a decreasing stress. According to the FEM results, the cell stress is mainly influenced by the strain in the backsheet for thin cells. For thicker solar cells (>110  $\mu\text{m}$ ), the influence of the backsheet vanishes, because the stiffness of the solar cell increases with its thickness. The turning point is visible by the nearly constant stress level between 100  $\mu\text{m}$  and 110  $\mu\text{m}$  cell thickness in figure 11.

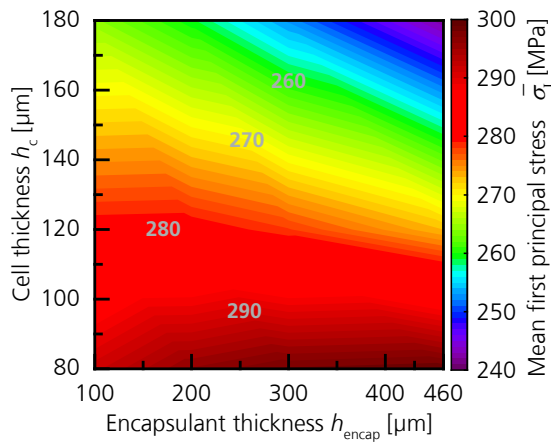


**Figure 11:** Mean first principal stress  $\bar{\sigma}_1$  on rear side of the solar cell of the model with EVA with ECAI at 2400 Pa pressure load for different encapsulant and solar cells thickness. All values are above the characteristic fracture stress  $\sigma_\theta$ .

However, all obtained stress values are far above the characteristic fracture stress  $\sigma_\theta$ . From prior studies it is known that a frame reduces the stress in the solar cells significantly [6]. Therefore we replace the clamps in the FEM model by a frame fixed at four positions, according to [6]. With this modified model we simulate for 200  $\mu\text{m}$  encapsulant and 80  $\mu\text{m}$  cell thicknesses the material combination with the lowest stress, namely EVA with ECAI. Additionally we investigate the potential of a glass-glass setup to reduce the stress by replacing the backsheet with a glass. For this setup the front glass has a thickness of 2 mm and the rear glass 2.035 mm, taking the electrically conductive copper layer into account. We simulate this setup with and without frame for EVA with ECAI. Due to the alteration of the mounting system, the FEM model of framed modules is not validated. However, since the mounting system is implemented in a sub-model of the laminate, the laminate itself,

particularly the mesh, is identical for both FEM models. Therefore, the modified FEM model can be considered as reasonable and the results are presented in figure 12.

As expected, the frame reduces the deflection of the module significantly by 54%. Also the mean first principal stress  $\bar{\sigma}_1$  in the solar cells is significantly reduced to 114 MPa, which is below the characteristic fracture stress. A further decrease is achieved by the glass-glass setup. Here the influence of the frame is not significant anymore with stress values of 67 MPa and 66 MPa for frameless and framed modules respectively. So the main impact is a reduction of the strain in the rear layer of the module.

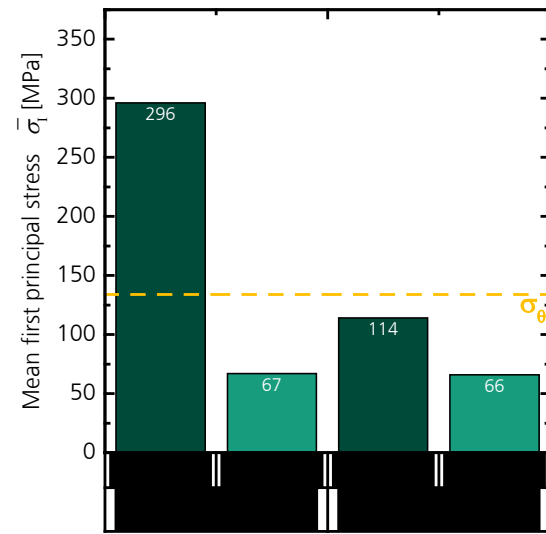


**Figure 12:** Mean first principal stress  $\bar{\sigma}_1$  on rear side of the solar cell (80  $\mu\text{m}$ ) of the model with 200  $\mu\text{m}$  EVA with ECAI at 2400 Pa pressure load for different module designs. The dashed yellow line indicates the characteristic fracture stress  $\sigma_\theta$ .

In conclusion ultra-thin back contact solar cells can be integrated in modules using thin encapsulants if either a glass-glass setup is chosen or a frame is used. In this study the characteristic fracture stress  $\sigma_\theta$  of the MWT-cells is rather low, comparing to standard solar cells with about 200 MPa [14]. So keeping in mind that the fracture stress might be higher for other back contact solar cell concepts, like IBC, ultra-thin solar cells can also be integrated into a framed glass-foil module using thin encapsulants.

#### 4 CONCLUSION

This paper presents a validated FEM model of a frameless 60-cell back contact module. We compare six different material combinations according to their impact on the tensile stress in the solar cells. We measure the temperature dependent Young's modulus of three encapsulants by a dynamic mechanical analyzer in order to capture their material behaviour properly. Additionally we measure their Poisson's ratio as well as the Young's modulus of the backsheet with a tensile testing machine. For all six material combinations we vary the thickness of the solar cells and the encapsulant in the FEM simulations. We obtain the lowest stress value (260 MPa) for 200  $\mu\text{m}$  thick EVA with ECAI and 180  $\mu\text{m}$  cells. Depending on the material combination,

the stress increases between 4% and 12% if the cell thickness is reduced to 80  $\mu\text{m}$ . Due to the electrical connection concept used, the stress dependency on the encapsulant thickness is different for cells below or above about 110  $\mu\text{m}$  thickness. For thin cells ( $< 110 \mu\text{m}$ ), the stress increases with increasing encapsulant thickness, while for thick cells the stress decreases.

For the combination of 200  $\mu\text{m}$  EVA, ECAI and 80  $\mu\text{m}$  cells, the stress is significantly reduced (296 MPa to 114 MPa) by using a frame instead of laminate clamps. A glass-glass setup reduces the stress even further to 67 MPa for clamped and 66 MPa for framed modules. With this the FEM simulations we show that it is possible to integrate ultra-thin back contact solar cells in a PV module.

#### 5 ACKNOWLEDGEMENT

This project has received funding from the European Union's Seventh Programme for research, technological development and demonstration under grant agreement No 609788, acronym CHEETAH and from the Cusanuswerk by a PhD-scholarship. The authors like to thank Li Carlos Rendler and Pascal Romer (both Fraunhofer ISE) for the fruitful discussions.

#### 6 REFERENCES

- [1] B. Klein, *FEM - Grundlagen und Anwendungen der Finite-Element-Methode im Maschinen- und Fahrzeugbau*, 9th ed. Wiesbaden, Germany: Vieweg+Teubner Verlag, 2012.
- [2] *IEC 61215: 2005-04. Crystalline silicon terrestrial photovoltaic (PV) modules - Design qualification and type approval*, 2005.
- [3] M. Meuwissen *et al.*, "Simulation assisted design of a PV module incorporating electrically conductive adhesive interconnects," in *Proc. of the 21st European Photovoltaic Solar Energy Conference and Exhibition*, 2006, pp. 2485–2490.
- [4] F. Kraemer, S. Wiese, E. Peter, and J. Seib, "Mechanical problems of novel back contact solar modules," *Microelectronics Reliability*, vol. 53, no. 8, pp. 1095–1100, 2013.
- [5] I. Bennett and N. Loiseaux, "Measurement of Strains in MWT Modules During Manufacture," *Proceedings of the 2nd International Conference on Crystalline Silicon Photovoltaics SiliconPV 2012*, vol. 27, no. 0, pp. 697–702, 2012.
- [6] A. J. Beinert, M. Ebert, U. Eitner, and J. Aktaa, "Influence of Photovoltaic Module Mounting Systems on the Thermo-Mechanical Stresses in Solar Cells by FEM Modelling," in *Proc. of the 32nd European Photovoltaic Solar Energy Conference and Exhibition*, München: WIP, 2016, pp. 1833–1836.
- [7] U. Eitner, S. Kajari-Schroeder, M. Koentges, and H. Altenbach, "Thermal stress and strain of solar cells in photovoltaic modules," in *Advanced Structured Materials*, vol. 15, *Shell-like Structures: Non-classical Theories and Applications*, H. Altenbach and V. A. Eremeyev, Eds, Berlin/Heidelberg: Springer, 2011.
- [8] R. B. Roberts, "Thermal expansion reference data: silicon 80-280K," *Journal of Physics D: Applied Physics*, vol. 15, no. 9, pp. L119, 1982.
- [9] R. B. Roberts, "Thermal expansion reference data: silicon 300-850 K," *Journal of Physics D: Applied Physics*, vol. 14, no. 10, pp. L163, 1981.
- [10] W.M. Haynes, Ed, *CRC handbook of chemistry and physics*: CRC Press, 2014.
- [11] W. Weibull, "A statistical distribution function of wide applicability," *Journal of Applied Mechanics*, vol. 18, pp. 293–305, 1951.
- [12] W. Weibull, *A Statistical Theory of the Strength of Materials*. Stockholm: Generalstabens Litografiska Anstalts Förlag, 1939.
- [13] M. Sander, A. Dietrich, M. Pander, M. Ebert, and J. Bagdahn, "Systematic investigation of cracks in encapsulated solar cells after mechanical loading," *Solar Energy Materials and Solar Cells*, vol. 111, pp. 82–89, 2013.
- [14] F. Kaule, W. Wang, and S. Schoenfelder, "Modeling and testing the mechanical strength of solar cells," *Solar Energy Materials and Solar Cells*, vol. 120, Part A, pp. 441–447, 2014.